



## BMCL Digest

## Substituted *N*-aryl-6-pyrimidinones: A new class of potent, selective, and orally active p38 MAP kinase inhibitors

Balekudru Devadas<sup>a,\*</sup>, Shaun R. Selness<sup>a</sup>, Li Xing<sup>b</sup>, Heather M. Madsen<sup>a</sup>, Laura D. Marrufo<sup>a</sup>, Huey Shieh<sup>b</sup>, Dean M. Messing<sup>c</sup>, Jerry Z. Yang<sup>d</sup>, Heidi M. Morgan<sup>e</sup>, Gary D. Anderson<sup>e</sup>, Elizabeth G. Webb<sup>e</sup>, Jian Zhang<sup>e</sup>, Rajesh V. Devraj<sup>a</sup>, Joseph B. Monahan<sup>e,†</sup>

<sup>a</sup> Department of Medicinal Chemistry, Pfizer Corporation, 700 Chesterfield Parkway West, Chesterfield, MO 63017, USA

<sup>b</sup> Structural and Computational Chemistry, Pfizer Corporation, 700 Chesterfield Parkway West, Chesterfield, MO 63017, USA

<sup>c</sup> Department of Pharmacokinetics and Drug Metabolism, Pfizer Corporation, 700 Chesterfield Parkway West, Chesterfield, MO 63017, USA

<sup>d</sup> Department of Pharmaceutical Sciences, Pfizer Corporation, 700 Chesterfield Parkway West, Chesterfield, MO 63017, USA

<sup>e</sup> Inflammation Biology, Pfizer Corporation, 700 Chesterfield Parkway West, Chesterfield, MO 63017, USA

## ARTICLE INFO

## Article history:

Received 5 February 2011

Revised 1 May 2011

Accepted 2 May 2011

Available online 8 May 2011

## Keywords:

p38 MAP kinase

Pyrimidinone

Tumor necrosis factor- $\alpha$

Oral bioavailability

Dual Hbond motif

Structure activity relationship

Dissolution rate

Anti-inflammatory

## ABSTRACT

A novel series of highly potent and selective p38 MAP kinase inhibitors was developed originating from a substituted *N*-aryl-6-pyrimidinone scaffold. SAR studies coupled with in vivo evaluations in rat arthritis model culminated in the identification of **10** with excellent oral efficacy. Compound **10** exhibited a significantly enhanced dissolution rate compared to **1**, translating to a high oral bioavailability (>90%) in rat. In animal studies **10** inhibited LPS-stimulated production of tumor necrosis factor- $\alpha$  in a dose-dependent manner and demonstrated robust efficacy comparable to dexamethasone in a rat streptococcal cell wall-induced arthritis model.

© 2011 Elsevier Ltd. All rights reserved.

p38 MAP kinase is a widely prosecuted disease target that has resulted in the discovery of a variety of inhibitor classes with diverse molecular architecture.<sup>1</sup> This enzyme plays a pivotal role in the MAP kinase signal transduction pathway resulting in the production of inflammatory cytokines including TNF- $\alpha$  and IL-1 $\beta$ .<sup>2</sup> Modulation of these cytokines by ATP-competitive small molecules has led to the generation of a variety of novel p38 inhibitors as potential therapeutics for the treatment of inflammatory conditions including Crohn's disease, psoriasis, and rheumatoid arthritis (RA).<sup>3</sup> Several of the p38 kinase inhibitors have advanced into human clinical trials, and our own efforts have led to the identification of a novel pharmacophore **1**, (Fig. 1) as a clinical candidate for RA.<sup>4,5</sup> This compound exhibits exceptional selectivity for p38 $\alpha$  (MAPK14) versus other kinases due to a unique binding mode involving a dual H-bond motif, engaging Met109 and Gly110 residues, with a flipped backbone conformation of Gly110

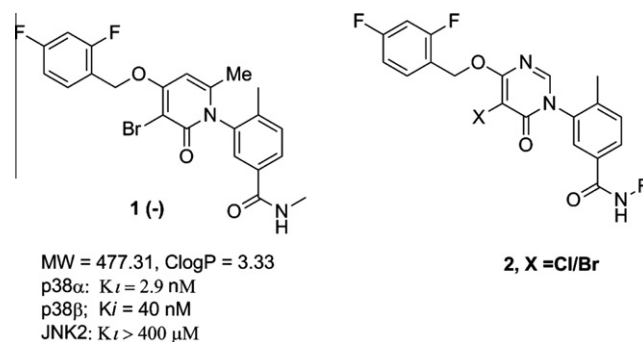


**Figure 1.** Structures of pyrimidinone and pyrimidinone classes of p38 kinase inhibitors.

from its apo state.<sup>6</sup> The backbone flip occurs in p38 $\alpha$  due to the presence of the glycine in the hinge region, which has no side chain and consequently has sufficient conformational flexibility to induce a peptide backbone flip. In the human kinome, only p38 $\beta$  and Myt-1 contain the corresponding glycine and a threonine at

\* Corresponding author.

E-mail address: [balekudru.devadas@yahoo.com](mailto:balekudru.devadas@yahoo.com) (B. Devadas).

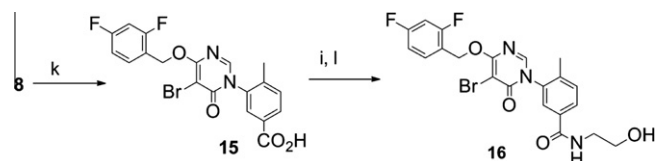
<sup>†</sup> Present address: Confluence Life Sciences, 4320 Forest Park Avenue, Suite 303, St. Louis, MO 63108, USA.

the gatekeeper position, which provides a structural rationale for the observed high level of selectivity.<sup>6</sup>

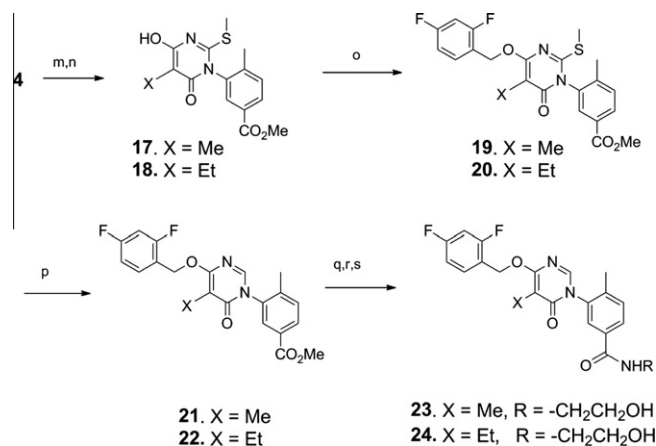
The 2-pyridinone lead **1** (aS atropomer), despite its excellent in vitro and in vivo activity profiles, suffers from poor solubility which could lead to dissolution-limited absorption and potential variability in oral bioavailability at projected clinical doses. Upon examination of the X-ray structure of the **1**-p38 complex,<sup>6</sup> it was evident that the *N*-methyl group is exposed to the solvent accessible region, which provided an opportunity to improve solubility and pharmacokinetic properties. Furthermore, **1** is optically active by virtue of its asymmetry introduced by restricted rotation around the C–N bond between the 2-pyridinone ring and the benzamide moiety. A chiral separation step is necessary for the isolation of the aS atropomer. In order to overcome these issues we initiated the synthesis of the corresponding pyrimidinone analogs with reduced lipophilicity bearing polar amide substituents, represented by **2**. This report discloses the synthesis, structure–activity relationship studies leading to the discovery of **10** as a clinical candidate, and the X-ray crystallographic structure of **10** bound to the ATP-binding site of the p38 enzyme.

As shown in Scheme 1, the synthesis of *N*-arylpurimidinones commenced with the formation of the 3-thioureidobenzoate precursor **4**, from methyl-3-amino-4-methylbenzoate **3** and potassium thiocyanate in the presence of 4 N HCl. The pyrimidinone ring was then assembled by the condensation of **4** with dimethylmalonate in the presence of sodium methoxide, followed by methylation, to afford the 2-thio-methyl-4-hydroxy intermediate **5**. Reaction of **5** with 2,4-difluorobenzyl chloride in the presence of potassium carbonate in *N*-methylpyrrolidine provided **6** in good yield.

Desulfurization of **5** using Raney Ni presented a synthetic challenge due to over-reduction of the pyrimidinone core and poor conversion to the desired product **7**. However, optimal conditions were established by carrying out the reaction in 2-propanol or dimethylacetamide at 60 °C to give the pyrimidinone derivative **7** in 80% yield. In the next step, ester **7** was converted to the corresponding acid **8** and subjected to chlorination using *N*-chlorosuccinimide in dichloroethane in the presence of catalytic amounts



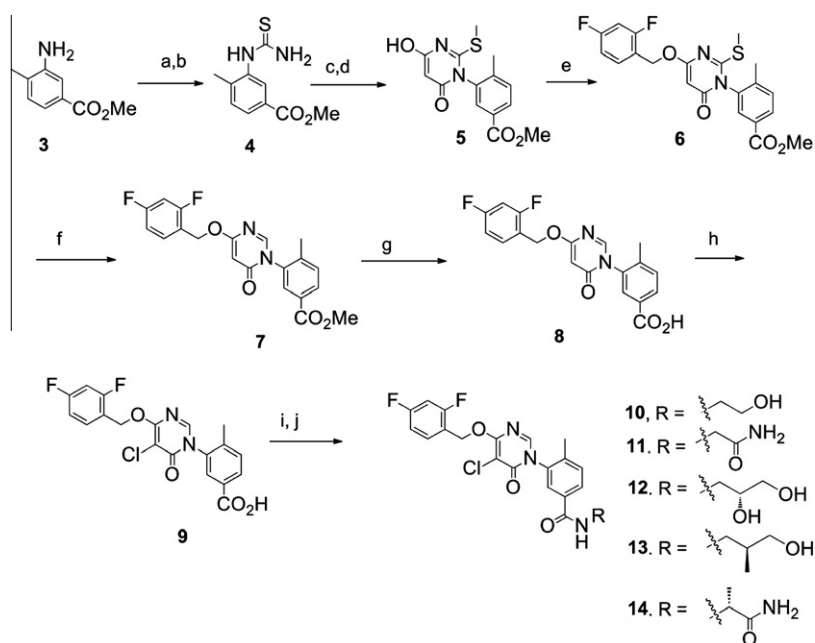
**Scheme 2.** Reagents and conditions: (k) NBS, dichloromethane, rt, 5 h; (i) isobutylchloroformate, *N*-methylmorpholine, DMA 0 °C to rt; (l) 2-aminoethanol.



**Scheme 3.** Synthesis of C-5-methyl/ethyl pyrimidinones. Reagents and conditions: (m) diethyl-2-alkyl-malonate, 25% NaOMe, 18-crown-6, dioxane, 70 °C; (n) MeI, rt; (o) 2,4-difluorobenzylbromide, K<sub>2</sub>CO<sub>3</sub>, DMF, rt, 12 h; (p) Raney Ni, 70 °C, DMA, 6 h; (q) 2 N NaOH, rt, citric acid; (r) 2 M Oxalyl chloride, DMF, DCM; (s) RNH<sub>2</sub>.

of dichloroacetic acid to provide **9**. The final compounds **10–14** were prepared by activation of **9** via the mixed anhydride formation, followed by coupling with amines.

Molecular modeling suggested a small hydrophobic pocket around the 5-position of the pyrimidinone ring. In order to assess its steric compatibility, the 5-bromo analog **16** was prepared in a



**Scheme 1.** Synthesis of 5-chloropyrimidinones. Reagents and conditions: (a) KSCN; (b) 4 N HCl, dioxane, 80 °C 20 h; (c) dimethylmalonate, NaOMe; (d) MeI; (e) 2,4-difluorobenzylchloride, K<sub>2</sub>CO<sub>3</sub> NMP rt; (f) Raney Ni, DMA, 80 °C 12 h; (g) 2 N NaOH, dioxane rt, 1 h, 5% citric acid; (h) NCS, dichloroacetic acid, dichloroethane, 65 °C; (i) isobutylchloroformate, *N*-methylmorpholine, DMA; (j) RNH<sub>2</sub>

similar manner as depicted in Scheme 2 using *N*-bromosuccinimide in place of *N*-chlorosuccinimide.

To further evaluate the role of steric and electronic effects at the 5-position, the synthesis of 5-methyl and 5-ethyl analogs **23** and **24** were undertaken as outlined in Scheme 3. Condensation of **4** with diethyl-2-methylmalonate in the presence of sodium ethoxide resulted in the formation of **17** in 87% yield. The corresponding ethyl derivative **18** was obtained in 94% yield under similar conditions.

In the next step, the 2,4-difluorobenzyl group was installed using 2,4-difluorobenzyl bromide in the presence of  $K_2CO_3$  to provide **19** and **20**. Raney Ni assisted desulfurization provided **21** and **22** in good yields. These were converted to the target compounds **23** and **24** following hydrolysis, acid chloride formation using oxalyl chloride, and coupling with 2-aminoethanol.

To understand the importance of the oxygen linker at the C-4 position to the p38 $\alpha$  binding affinity, preparation of the 4-thio analog **29** was also carried out as depicted in Scheme 4. The aniline ester **3** was converted to the cyanoacetamide precursor **25**. Treatment of **25** with diethyldithiophosphate furnished **26** in 90% yield. Subsequent cyclization of **26** with methylformate followed by installation of the 2,4-difluorobenzyl group provided **27**.

Following the conversion of **27** to its acid derivative, chlorination was carried out to furnish **28**. Activation of the carboxyl group in **28** by conversion to the acid chloride and exposure to 2-aminoethanol afforded the final compound **29**.

These new analogs **10–14**<sup>7</sup> in general showed good potency against p38 $\alpha$ <sup>8</sup> and in vitro metabolic stability.<sup>9</sup> Although the diol

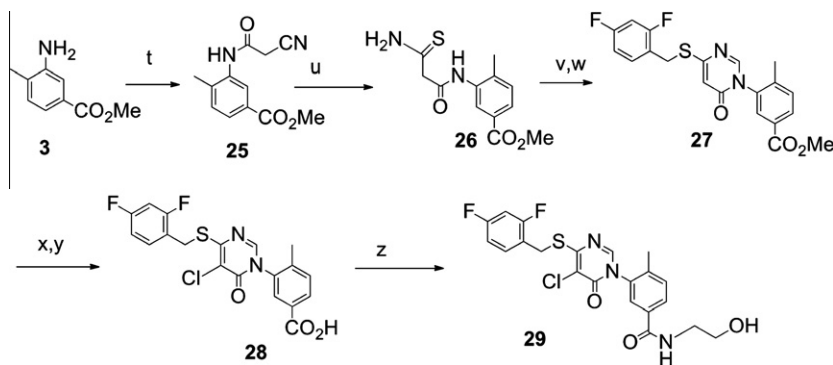
**12** and the amide **14** exhibited improved solubility<sup>10</sup> compared to the hydroxyl-substituted compounds **10** and **13**, they showed significantly higher efflux ratios as measured by Caco-2 cell permeability. While the amide analog **11** maintained excellent potency against p38 $\alpha$  it suffered from poor aqueous solubility. Unlike the chloro analog **10**, the corresponding bromo counterpart **16** was found to be less soluble and less potent against p38 $\alpha$  ( $IC_{50}$  = 60 nM). Like **1**, these substituted 6-pyrimidinones were found to be highly selective versus JNK2 ( $IC_{50}$  >200  $\mu$ M).

In an effort to expand the structural diversity of this class of inhibitors, we synthesized the 5-methyl and 5-ethyl analogs **23** and **24**, respectively. While these maintained good potency against p38 $\alpha$  and good inhibition of LPS-induced TNF- $\alpha$  production (Table 2, we de-prioritized this series due to low aqueous solubility.

The prominent role played by the oxygen linker is revealed by the sulfur analog **29**, which exhibited significantly decreased potency ( $IC_{50}$  = 193 nM) to p38 $\alpha$ .

Due to the superior potency ( $K_i$  = 6.4 nM) and low efflux ratio displayed by **10**, it was further evaluated in cellular assays and in vivo disease models of inflammation.<sup>11,12</sup> The cellular potency of **10** correlated well with its inhibition of recombinant enzyme activity, consistent with a p38 kinase mechanism of action (Table 1).

The U937 cellular activity of **10** (Table 3)<sup>8</sup> was confirmed and extended using LPS-stimulated human monocytes and human whole blood. In human monocytes, LPS-stimulated production of TNF- $\alpha$  and IL-1 $\beta$  was inhibited by **10** with an  $IC_{50}$  of 25.6 nM and



**Scheme 4.** Synthesis of 4-thio analog. (t) methylcyano acetate, DBU, xylene, reflux, 42%; (u) diethyldithiophosphate, dioxane/water, 80 °C 24 h, 74%; (v) methylformate, sodium methoxide; (w) 2,4-difluorobenzylbromide,  $K_2CO_3$ , rt; (x) *N*-chlorosuccinimide, *i*-propanol, reflux, 20 min; (y) 2 N NaOH, dioxane, rt; (z) Oxalyl chloride, DMF, 2-aminoethanol. Following the conversion of **27** to its acid derivative, chlorination was carried out to furnish **28**. Activation of the carboxyl group in **28** by conversion to the acid chloride and exposure to 2-aminoethanol afforded the final compound **29**.

**Table 1**  
In vitro potency, metabolic stability, and in vivo activity of 5-chloro-substituted-6-pyrimidinones

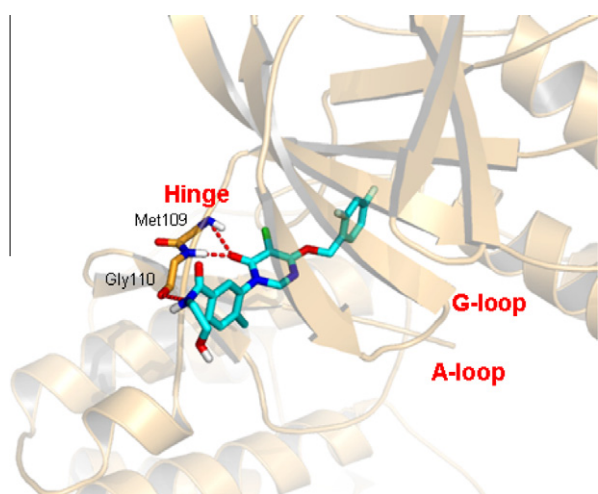
Compound #	p38 $\alpha$ $IC_{50}$ ( $\mu$ M)	Met. stab. (% remaining)	Rat LPS (%) Inh. of TNF $\alpha$ @ 5 mpk	Aq solubility (amorphous, @pH 6.5, $\mu$ g/mL)	Caco-2 Cell efflux ratio	Rat SCW (% Inh. of disease score @30mpk/day)
<b>10</b>	0.029	99 (Human) 97 (Rat)	95.2	51	4.2	94.8
<b>11</b>	0.03	100 (Human) 100 (Rat)	84.3	14	ND	ND
<b>12</b>	0.027	97 (Human) 100 (Rat)	91.5	163	32.8	ND
<b>13</b>	0.012	96 (Human) 85 (Rat)	91.3	94	7.5	82.4
<b>14</b>	0.006	77 (Human) 72 (Rat)	92.9	147	23.6	ND

**Table 2**  
In vitro potency, metabolic stability, and in vivo activity of 5-methyl/ethyl-substituted-6-pyrimidinones

Compound #	R	p38 $\alpha$ $IC_{50}$ ( $\mu$ M)	p38 $\alpha$ $K_i$ ( $\mu$ M)	JNK2 $IC_{50}$ ( $\mu$ M)	Met. Stab. (% Remaining)	Aq. solubility (Amorphous, @pH 6.5, $\mu$ g/mL)	Rat LPS (%) Inh. of TNF $\alpha$ @ 5 mpk
<b>23</b>	Methyl	0.038	0.017	>200	84 (Human) 99 (Rat)	28	94.7
<b>24</b>	Ethyl	0.011	0.006	>200	76 (Human) 92 (Rat)	20	91.8

**Table 3**  
Cellular activity of **10** and **1** on cytokine production and p38 activity

Assay	Compound <b>10</b>	Compound <b>1</b>
U937 TNF $\alpha$ IC <sub>50</sub> (nM)	35.5 $\pm$ 18.8	5.9 $\pm$ 1.3
U937 p38 kinase activity IC <sub>50</sub> (nM)	12.0 $\pm$ 1.2	1.05 $\pm$ 0.64
Human Monocyte TNF $\alpha$ IC <sub>50</sub> (nM)	25.6 $\pm$ 4.3	3.4 $\pm$ 2.0
Human Monocyte IL-1 $\beta$ IC <sub>50</sub> (nM)	37.2 $\pm$ 6.5	3.4 $\pm$ 0.5
Human Monocyte p38 kinase activity IC <sub>50</sub> (nM)	16.9 $\pm$ 3.4	17.4 $\pm$ 6.9
Human Whole Blood TNF $\alpha$ IC <sub>50</sub> (nM)	177 $\pm$ 30	85 $\pm$ 21

**Figure 2.** Crystal structure of **10** bound to active site of p38 $\alpha$ . Crystals of p38 $\alpha$ -**10** complex were obtained by soaking experiment. The structure has been refined to a  $R_{\text{free}}$  of 27.6% at 1.7Å ( $R_{\text{crystal}} = 23.9\%$ ). The inhibitor is represented with carbon, nitrogen, oxygen and chlorine in cyan, blue, red, and green respectively. The hydrogen bonds are shown by dotted red lines.**Table 4**  
In vivo efficacy of **10** and **1** in acute & chronic inflammation models

Assay	Compound <b>10</b> ED <sub>50</sub> /ED <sub>80</sub> (mg/kg)	Compound <b>1</b> ED <sub>50</sub> /ED <sub>80</sub> (mg/kg)
Rat LPS induced TNF $\alpha$ inhib.	0.115/0.259	0.07/0/142
Rat SCW Arthritis	0.105/0.649	0.186/1.61

37.2 nM respectively, while in the whole blood assay, TNF- $\alpha$  synthesis was inhibited with an IC<sub>50</sub> value of 177 nM. This lower potency of **10** is consistent with its plasma protein binding

**Table 5**  
Summary of PK parameters for **10**

Species	Dose (mg/kg)	CL (ml/min/kg)	V <sub>dss</sub> (L/kg)	t <sub>1/2</sub> (h)	Oral BA (%)
Rat (IV)	0.2	3.19	1.32	6.5	
Rat (PO)	0.2				99%
Dog (IV)	1	1.59	0.986	8.7	
Dog (PO)	1				67%

**Table 6**  
Effect of dissolution rate on BA

Compound	Solid State	Solubility (pH 6.5 $\mu$ g/mL)	Intrinsic Dissolution Rate ( $\mu$ g/min/cm <sup>2</sup> )	logP	Permeability P <sub>app</sub> 10 <sup>-6</sup> cm/s, (Efflux Ratio)	Rat Oral Dose (mpk)	Rat Oral BA (suspension)
<b>1</b>	Crystalline	~10	0.3	3.35	15.9 (4.4)	5	9.3 $\pm$ 3.2%
<b>10</b>	Crystalline (Form A)	23	6.1	1.65	7.99 (4.4)	5	99%

(96.3%) characteristics. While **10** was shown to inhibit cellular p38 kinase activity as assessed by p38 kinase dependent phosphorylation of HSP-27, no inhibition of the JNK or ERK pathways was observed in U937 cells at a concentration of 1  $\mu$ M.

The crystallographic data (Fig. 2) revealed that **10** binds in the ATP binding site of p38 $\alpha$ , with a characteristic dual H-bond motif, engaging both Met109 and Gly110 residues.<sup>13</sup> In analogy to the pyridinone inhibitor **1**, the backbone flip of Gly110 was observed with **10**. The 2,4-difluorobenzyloxy group occupied the lipophilic pocket defined by Thr106 as the gatekeeping residue. The *N*-phenyl group is directed toward the solvent front. Similar to the binding mode of **1**, the binding conformation of the benzamide moiety in **10** is driven by the polar interaction between its amide NH and the backbone carbonyl of Gly110. Although **10** is devoid of the 2-methyl substitution in the pyrimidinone core, it exhibits orthogonal geometry between *N*-phenyl and the pyrimidinone ring, a binding conformation that is driven by the stacking of the *N*-phenyl onto the peptide backbone of Gly110-Ala111.<sup>5</sup>

In vivo pharmacological evaluations of **10** were carried out both in acute and chronic disease models of inflammation. In a rat LPS model, with a 4 h oral pre-dosing interval regimen, all compounds showed a dose-dependent inhibition of LPS stimulated TNF- $\alpha$  production.<sup>11</sup> Compound **10** was found to be the most efficacious candidate in this series, with an ED<sub>50</sub> value of 0.115 mg/kg and ED<sub>80</sub> of 0.259 mg/kg. Based on the superior in vitro and in vivo profiles, **10** was further evaluated in the chronic SCW-arthritis model.

Analogue **10** was found to be highly effective in mitigating SCW-induced inflammation (Table 4).<sup>12</sup> It showed a dose-dependent inhibition of paw swelling when administered from 10 to 21 days with ED<sub>50</sub> and ED<sub>80</sub> values of 0.105 mg/kg and 0.649 mg/kg b.i.d. respectively. Anti-inflammatory effects observed with **10** were comparable to that achieved with dexamethasone. Furthermore, it was observed that **10** protected ankle joint as evidenced by retention of bone integrity measured by  $\mu$ CT analysis. Cellular studies suggested that the mechanism by which **10** displayed bone protective effect may be through the inhibition of osteoclast differentiation, a cell type primarily responsible for bone resorption.<sup>14</sup>

**10** was evaluated for its pharmacokinetic (PK) properties in rat and dog. The oral bioavailability (BA) was 99% and 67% in rat and dog respectively (Table 5). **10** exhibited low clearance and moderate volume of distribution in both species. The primary contributor for the observed superior bioavailability for **10** across species appears to be due to a 20-fold increase in dissolution rate compared to **1** (Table 6).<sup>15</sup> A combination of low clearance with moderate volume of distribution and excellent oral bioavailability for **10** predicts human PK properties suitable for q.d. or b.i.d dosing regimen.

In summary we have identified a novel class of potent and selective p38 kinase inhibitors, originating from an *N*-aryl-6-pyrimidinone scaffold. Compound **10** displayed exquisite kinase selectivity for p38 $\alpha$  versus a panel of over 100 related kinases.<sup>16</sup> It blocked LPS-induced TNF- $\alpha$  production in human monocyte and showed robust efficacy and target modulation in rat LPS and SCW arthritis models. The efficacy seen in these models appears to be driven by down regulation of p38 kinase activity because **10** did not cross over to parallel signaling pathways as measured by cellular assays. Furthermore, **10** demonstrated remarkable anti-inflammatory and joint protective activity in rodent chronic disease models. A dose-dependent inhibition of mechanism biomarkers was achieved upon oral dosing of **10**. On the basis of superior pharmacodynamic and pharmacokinetic profiles, **10** was selected for evaluation in humans.

### Acknowledgement

We thank Sean Juo for technical assistance in obtaining the PDB deposition number.

### References and notes

- (a) Saklatvala, J. *Curr. Opin. Pharm.* **2004**, 4(4), 372; (b) David, J. D.; Tsung, H. L. *Curr. Topics in Med. Chem.* **2005**, 5, 953.
- (a) Adams, J. L.; Badger, A. M.; Kumar, S.; Lee, J. C. *Prog. Med. Chem.* **2001**, 38, 1; (b) Dinarello, C. A. *Curr. Opin. Immunol.* **1991**, 3, 941.
- Kumar, S.; Boehm, J.; Lee, J. C. *Nat. Rev. Drug. Discovery* **2003**, 717–726.
- Selness, S. R.; Devraj, R. V.; Monahan, J. B.; Boehm, T. L.; Walker, J. K.; Devadas, B.; Durley, R. C.; Kurumbail, R.; Shieh, H.; Xing, L.; Hepperle, M.; Jerome, K. D.; Benson, A. G.; Marrufo, L. D.; Madsen, H. M.; Hitchcock, J.; Owen, T. J.; Christie, L.; Promo, M. A.; Hickory, B. S.; Alvira, E.; Naing, W.; Blevis-Bal, R. *Bioorg. Med. Chem. Lett.* **2009**, 19, 5851.
- Hope, H. R.; Anderson, G. D.; Burnette, B. L.; Compton, R. P.; Devraj, R. V.; Hirsch, J. L.; Keith, R. H.; Li, X.; Mbalaviele, G.; Messing, D. M.; Saabye, M. J.; Schindler, J. F.; Selness, S. R.; Stillwell, L. L.; Webb, E. G.; Zhang, J.; Monahan, J. B. *J. Pharm. Exp. Therap.* **2009**, 331(3), 882.
- Xing, L.; Shieh, H. S.; Selness, S. R.; Devraj, R. V.; Walker, J. K.; Devadas, B.; Hope, H. R.; Compton, R. P.; Schindler, J. F.; Hirsch, J. L.; Benson, A. G.; Kurumbail, R. G.; Stegeman, R. A.; Williams, J. M.; Broadus, R. M.; Walden, Z.; Monahan, J. B. *Biochemistry* **2009**, 48, 6402.
- All compounds showed <sup>1</sup>H NMR and mass spectra consistent with their structure and were > 95% purity by HPLC.
- Durley, R. C.; Devadas, B.; Madsen, H. M.; Hickory, B. S.; Palmquist, K.; Selness, S. R. WO 2004087677.
- Metabolic stability was determined in vitro by incubating 2  $\mu$ M test compound with human or rat liver microsomes, NADPH and buffer at 37 °C for 45 min and measuring percent compound remaining by a precipitation procedure followed by LC–MS analysis.
- Aqueous solubility is expressed in  $\mu$ g/mL at pH 6.5.
- Adult male Lewis rats (Harlan Sprague Dawley, Indianapolis, IN) (225–250 g) were used in these studies. Rats were fasted 18 h prior to oral dosing, and allowed free access to water throughout the experiment. Each treatment group consisted of five animals. **10** was prepared as a suspension in a vehicle consisting of 0.5% methylcellulose, (Sigma, St. Louis, MO), 0.025% Tween 20 (Sigma). The compound or vehicle was administered by oral gavage in a volume of 1 mL. Two vehicle groups were used per experiment to control for intra-experiment variability, and three experiments were performed. LPS (*E. coli* serotype 0111:B4, Sigma) was administered four hours later by intravenous injection at a dose of 1 mg/kg in 0.5 mL sterile saline (Baxter Healthcare, Deerfield, IL). Blood was collected in serum separator tubes via cardiac puncture ninety minutes after LPS injection, a time point corresponding to maximal TNF $\alpha$  production (data not shown). After clotting, serum was withdrawn and stored at –20 °C until it was assayed for TNF $\alpha$ . TNF $\alpha$  levels in serum were quantified from a recombinant rat TNF $\alpha$  (Biosource International) standard curve using a four parameter fit generated by an Excel (Microsoft, Redmond, WA) macro. The limit of detection for the ELISA was approximately 41 pg TNF $\alpha$ /mL.
- 10** was assayed in Streptococcal Cell Wall(SCW) induced Arthritis in Rats as follows: Arthritis was induced in female Lewis rats by a single intraperitoneal administration of peptidoglycan-polysaccharide complexes isolated from group a SCW (15  $\mu$ g/g bodyweight). The SCW preparation was purchased from Lee Labs. (Grayson, GA). The disease course is biphasic in which an acute inflammatory arthritis develops within days 1–3 (non-T-cell-dependent phase) followed by a chronic erosive arthritis (T-cell- dependent phase) developing on days 14–28. Only animals developing the acute phase were treated with **10** from days 10 to 21 after SCW injection. Paw volume was measured on day 21 by using a water displacement plethysmometer. **10** was prepared as an aqueous suspension in 0.5% methylcellulose and 0.025% Tween 20(Sigma–Aldrich). It was administered by oral gavage in a volume of 0.5 mL beginning on day 10 post-SCW injection and continuing daily until day 21. Animals were dosed between 0.015 and 5 mg/kg b.i.d. with **10**. Methylcellulose/Tween 20 vehicle was used for comparison. Group size was four to eight animals per group. Two paw volumes were taken for each animal. Paw volume was measured on day 21 by using a water displacement plethysmometer. Three to four paws from each treatment group were scanned for bone density evaluation. Plasma samples were collected on day 21 for determination of compound levels.
- The coordinates of compound **10** bound to p38 have been deposited with the Protein Data Bank and assigned RCSB ID code rcsb065177 and PDB ID code 3ROC.
- Treatment of rat bone marrow cells with **10** resulted in a dose-dependent inhibition of osteoclast formation induced by RANKL with an IC<sub>50</sub> of 10.1 nM.
- (a) Horter, D.; Dressman, J. B. *Adv. Drug Deliv. Rev.* **2001**, 46, 75; (b) Intrinsic Dissolution Rate = Initial Influx/ Total Surface Area of Rotating Disk.
- Compound **10** exhibited an IC<sub>50</sub> of >10  $\mu$ M for the following kinases: JNK1, JNK2, JNK3, ERK2, PRK, MK2, MK3, MKK6, CDK2, IKK1, IKK2, Aurora-A, Myt1, ALK, TBK, BTK, CK1, CHK2, EGFR, FIt3, Lyn, MAPK1, MEK1, MKK4, MST2, ROCK II, Syk, Tie-2, MKK7, ZAP70, and inhibited p38 $\beta$  with an IC<sub>50</sub> of 0.249  $\mu$ M.